Accepted Manuscript

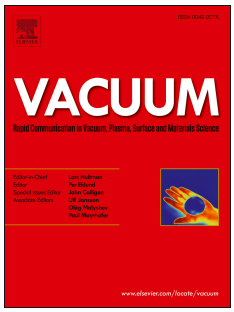

Modeling the effect of defects on the performance of an n-CdO/p-Si solar cell

S. Chala, N. Sengouga, F. Yakuphanoglu

PII: S0042-207X(15)00239-0

DOI: 10.1016/j.vacuum.2015.05.019

Reference: VAC 6681

To appear in: *Vacuum*

Received Date: 29 October 2014

Revised Date: 23 April 2015

Accepted Date: 18 May 2015

Please cite this article as: Chala S, Sengouga N, Yakuphanoglu F, Modeling the effect of defects on the performance of an n-CdO/p-Si solar cell, *Vaccum* (2015), doi: 10.1016/j.vacuum.2015.05.019.

This is a PDF file of an unedited manuscript that has been accepted for publication. As a service to our customers we are providing this early version of the manuscript. The manuscript will undergo copyediting, typesetting, and review of the resulting proof before it is published in its final form. Please note that during the production process errors may be discovered which could affect the content, and all legal disclaimers that apply to the journal pertain.

- The measured J-V characteristics are accurately reproduced by numerical simulation under different illumination intensities .

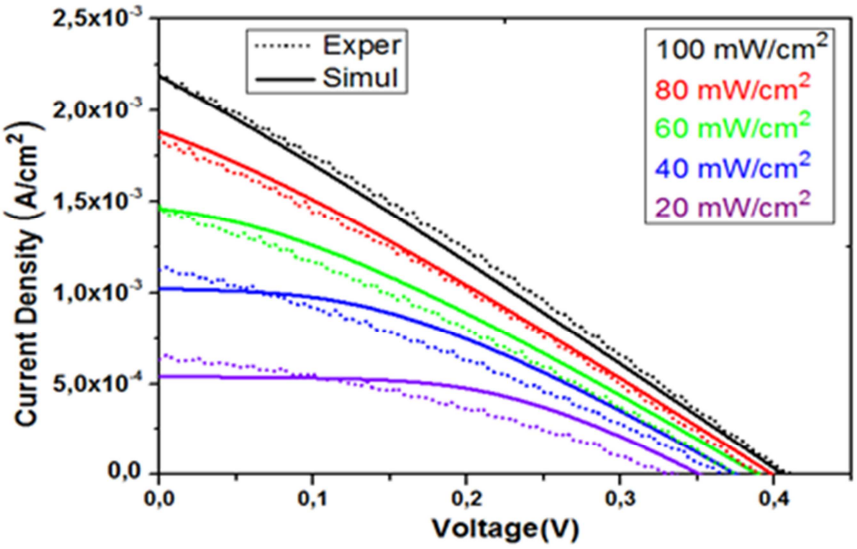

ACCEPTED MANUSCRIPT

ACCEPTED MANUSCRIPT

Modeling the effect of defects on the performance of an n-CdO/p-Si solar cell

S. Chala[a], N. Sengouga[a,*] and F. Yakuphanoglu[b]

[a]Laboratory of Metallic and Semiconducting Materials, Université de Biskra, 07000 Biskra, Algeria

[b]Physics Department, Firat University, 23169 Elazig, Turkey

[*]Corresponding author: n.sengouga@univ-biskra.dz (N Sengouga), Tel/Fax +213 33 54 31 99

Abstract

The interest in the study of Cadmium oxide (CdO) for photonic applications has increased significantly because of its promising electrical and optical properties. Real solar cells based on an n-CdO/p-Si heterostructures show poor photovoltaic performance, however. In this work numerical simulation is used to elucidate this poor performance by considering two cases. CdO is firstly considered as a perfect crystalline semiconductor. The second case models CdO as a semiconductor with continuous distribution of defects states in its band gap, similar to an amorphous semiconductor, made of two tail bands (a donor-like and an acceptor-like) and two Gaussian distribution deep level bands (an acceptor-like and a donor-like). Evidently the first case produced results far from reality. In the second case, however, and by adjusting the constituents of the band gap states the open circuit voltage (V_{OC}) and the short circuit current (J_{SC}) were almost perfectly reproduced but not the fill factor (FF) and the conversion efficiency (η). The p-type doping of Silicon adjustment has lead to a better reproduction of the two latter parameters.

ACCEPTED MANUSCRIPT

Keywords: CdO/Si solar cell; Characterisation; Simulation; Defects

1-INRODUCTION

Transparent conducting metal oxides (TCOs) have excellent transparency in the visible region as well as a high electrical conductivity. They are widely used as windows in solar cells. Indium tin oxide (ITO) is currently the most important TCO, but it suffers from some drawbacks such as the high cost of indium, weak optical absorption in the blue-green region, as well as chemical instability. Alternatives to ITO include Cadmium Oxide (CdO) which has high transparency in visible and near infrared (NIR) spectral regions as well as high electrical conductivity of pure and doped films [1-4]. Pure CdO has n-type degenerate semiconducting behaviour with relatively low electrical resistivity (10^{-2}–10^{-4} Ωcm; a direct bandgap of 2.2–2.7 eV and two indirect bandgaps of 1.18–1.2 eV and 0.8–1.12 eV. The high electrical conductivity of CdO results mainly from stoichiometric deviation and even without doping due to the existence of shallow donors caused by intrinsic interstitial cadmium atoms and oxygen vacancies. These also may give rise to some defects in CdO films which are usually point defects, which can be either interstitial Cadmium atom [5], Oxygen vacancy [6] or a residual hydrogen atom [7]. Its electrical conductivity can be improved by doping using a variety of elements such as Aluminum (Al), Copper (Cu), Iron (Fe); Silver (Ag), Tin (Sn), to name but a few [8-10]. It is also relatively cheaper to prepare using a wide variety of simple methods such as metalorganic chemical vapor deposition [11], pulsed laser deposition [12], sol-gel (spin coating, dip coating) [13], dc magnetron reactive sputtering [14] and spray based techniques [15-16]. In addition to TCOs, CdO is used in many device applications such as sensors [17], photodetectors [18], Schottky diodes [19], bipolar transistors [20] and solar cells [21-24].

n-CdO/p-Si heterojunction solar cell which was fabricated by sol–gel method shows poor photovoltaic performance [21]. In this work numerical simulation using Silvaco ATLAS software is used to model the aforementioned solar cell and to elucidate this poor performance.

3. Structure:

The semiconductor used to fabricate the diode in this study was p-type single crystal silicon with a thickness of 600 µm, and a resistivity of 5–10 Ωcm. CdO film was deposited on p-type-silicon by sol–gel dip coating method. The thickness of the CdO film was determined to be 187 nm using atomic force microscopy. Al metal front contacts were formed on CdO film in the form of circular dots of 2 mm in diameter and 100 nm in thickness. The back ohmic contact was formed by evaporating Al metal on the back of Si wafer. The cross-section of Al/ n-CdO/ p-Si/Al diode is shown in Figure 1. It has to be mentioned that the CdO film plays a double role: as a TCO window as well as the emitter of the n-p junction. Further details of the fabrication process and electrical and optical characterization of the solar cell material and device can be found in [21].

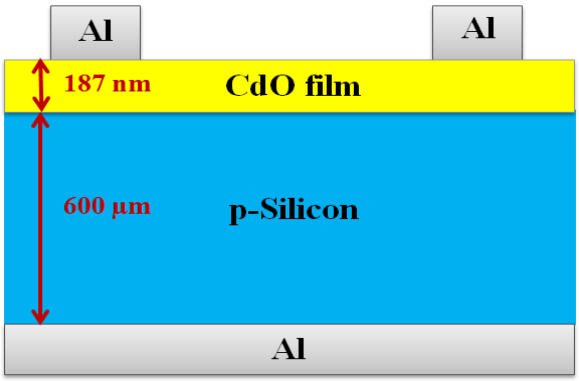

Figure 1.

4. Results and discussions

4.1. Solar cell J-V characteristics:

The photocurrent density-voltage characteristics of the solar cell were measured under different illumination intensities. Although these measurements were presented in [21] they will be later compared to simulation. In summary, the best values of Voc and Jsc of Al/ n-CdO/ p-Si/Al solar cell were found to be $V_{OC} = 0.41\ V$ and $J_{SC} = 2.19\ mA/cm^2$ under AM1.5, respectively. Although there are similar devices that show better performances in the literature [22-25], the main purpose of this work is to find the origin of the bad performance.

This poor performance was related to the presence of defects which create continuous distribution of trapping centers in the gap of CdO [26]. In the simulation section we will demonstrate this fact by considering the structure with and without the presence of the defects.

4.2. Simulation

The reliability and validity of simulation results must be performed by comparing them with those obtained in experimental studies. Otherwise, obtained simulation results are undermined and called into question, and it is neither possible nor feasible to re-use them in constructing real devices such as solar cells. In this respect parameters to be used in the simulation have to be published data from literature. Furthermore these data, if necessary have to be adjusted in a reasonable way, to yield simulation results comparable to measurements. The SILVACO TCAD ATLAS software was used [27] in this work to elucidate the poor performance of the Al/ n-CdO/ p-Si/Al solar cell. It is a physically-based two and three dimensional device simulator. It predicts the electrical

behavior of a specified structure and the internal physical mechanisms involved. It solves a set of fundamental equations, which link together the electrostatic potential and the carrier densities, through Poisson's equation, the carrier continuity equations and the transport equations. The simplest model of charge transport that is useful is the Drift-Diffusion Model [28]. The Poisson's equation which relates the electrostatic potential to the space charge density is given by:

$$div(\varepsilon \nabla \psi) = -\rho \tag{1}$$

where ψ is the electrostatic potential, ε is the local permittivity, and ρ is the local space charge density.

The space charge density in amorphous semiconductors (like CdO in the present work) is given by

$$\rho = q(p - n + n_{tail} - p_{tail} + n_{ga} - p_{gd} + N_d) \tag{2}$$

where *n* and *p* are the free carrier's densities, N_d is the n channel doping concentration and n_{tail}, p_{tail}, n_{ga}, p_{gd} are given by:

$$n_{tail} = \int_{E_v}^{E_c} g_{ct}^{A}(E) f_{ct}^{n}(E)\, dE$$

$$p_{tail} = \int_{E_v}^{E_c} g_{vt}^{D}(E) f_{vt}^{p}(E)\, dE$$

$$n_{ga} = \int_{E_v}^{E_c} g_{G}^{A}(E) f_{AG}^{n}(E)\, dE$$

$$p_{gd} = \int_{E_v}^{E_c} g_{G}^{D}(E) f_{DG}^{p}(E)\, dE$$

where $f_{ct}^{n}(E)$, $f_{AG}^{n}(E)$ are the ionization probabilities of the acceptor tail and Deep levels with Gaussian distribution, respectively, and $f_{vt}^{p}(E)$, $f_{DG}^{p}(E)$ are the ionization of

the donor states. At the steady state, these ionization probabilities are given by the Shockley-Read-Hall model as [29, 30]:

$$f_{ct}^{n}(E) = \frac{v_{th}^{n}\sigma_{nc}n + v_{th}^{p}\sigma_{pc}n_i e^{\frac{E_i - E}{k_B T}}}{v_{th}^{n}\sigma_{nc}\left(n + n_i e^{\frac{E - E_i}{k_B T}}\right) + v_{th}^{p}\sigma_{pc}\left(p + n_i e^{\frac{E_i - E}{k_B T}}\right)}$$

$$f_{AG}^{n}(E) = \frac{v_{th}^{n}\sigma_{ng}^{a}n + v_{th}^{p}\sigma_{pg}^{a}n_i e^{\frac{E_i - E}{k_B T}}}{v_{th}^{n}\sigma_{ng}^{a}\left(n + n_i e^{\frac{E - E_i}{k_B T}}\right) + v_{th}^{p}\sigma_{pg}^{a}\left(p + n_i e^{\frac{E_i - E}{k_B T}}\right)}$$

$$f_{vt}^{p}(E) = \frac{v_{th}^{p}\sigma_{pv}p + v_{th}^{n}\sigma_{nv}n_i e^{\frac{E - E_i}{k_B T}}}{v_{th}^{n}\sigma_{nc}\left(n + n_i e^{\frac{E - E_i}{k_B T}}\right) + v_{th}^{p}\sigma_{pc}\left(p + n_i e^{\frac{E_i - E}{k_B T}}\right)}$$

$$f_{DG}^{p}(E) = \frac{v_{th}^{p}\sigma_{pg}^{d}p + v_{th}^{n}\sigma_{ng}^{d}n_i e^{\frac{E - E_i}{k_B T}}}{v_{th}^{n}\sigma_{ng}^{d}\left(n + n_i e^{\frac{E - E_i}{k_B T}}\right) + v_{th}^{p}\sigma_{pg}^{d}\left(p + n_i e^{\frac{E_i - E}{k_B T}}\right)}$$

where v_{th}^{n} is the electron thermal velocity and v_{th}^{p} is the hole thermal velocity, n_i is the intrinsic carrier concentration. σ_{nc} and σ_{ng}^{a} are the electron capture cross-section for the acceptor states and deep levels with Gaussian distribution respectively. σ_{pc} and σ_{pg}^{a} are the hole capture cross-sections for the acceptor states and deep levels with Gaussian distribution respectively and σ_{nv}, σ_{ng}^{d}, σ_{pv}, and σ_{pg}^{d} are the equivalents for donors states. It has to be mentioned here that when Eq. 2 is applied to a crystalline semiconductor (like Si) the terms $n_{tail} - p_{tail} + n_{ga} - p_{gd}$ are neglected.

The continuity equations for both electrons and holes, in steady state, are expressed as:

$$\frac{\partial n}{\partial t} = \frac{1}{q} div\overrightarrow{J_n} + G_n - R_n \tag{3.a}$$

$$\frac{\partial p}{\partial t} = -\frac{1}{q} div\overrightarrow{J_p} + G_p - R_p \tag{3.b}$$

ACCEPTED MANUSCRIPT

where $\overrightarrow{J_n}$and $\overrightarrow{J_p}$ are the electron and hole current densities, G_n and G_p are the generation rates for electrons and holes, R_n and R_p are the total recombination rates for electrons and holes in deep and shallow states, and q is the electron charge. The generation rate of these pairs at a position *x* from the illuminated front is given by [31]:

$$G(x) = \int_{Spectrum} T(\lambda)\phi_0(\lambda)\alpha(\lambda)exp(-\alpha(\lambda)x)\, d\lambda \quad (4)$$

$T(\lambda)$ is the transmittance of the cell's top surface (CdO film), calculated for normal incidence by [31]:

$$T(\lambda) = 1 - R(\lambda) = 1 - \frac{(n(\lambda)-1)^2+k(\lambda)^2}{(n(\lambda)+1)^2+k(\lambda)^2} \quad (5)$$

where $R(\lambda)$ is the reflectivity, $n(\lambda)$ and $k(\lambda)$ are, respectively, the refractive index and the extinction coefficient of the CdO film. $\phi_0(\lambda)$ is the AM1.5 spectrum flux, $\alpha(\lambda)$ is the absorption coefficient. The refractive index *n* and extinction coefficient *k* of CdO with Eg=2,27 eV were extracted from transmittance and reflectance curves [32] using Eq.5.

R_n and R_p are assumed to be the same and given by [33]

$$R_n = R_p = \int_{E_V}^{E_C} (np - n_i^2)\left\{\left[\frac{v_{th}^n v_{th}^p \sigma_{pc}\, \sigma_{nc} g_{ct}^A(E)}{v_{th}^n \sigma_{nc}\left(n + n_i e^{\frac{E-E_i}{k_BT}}\right) + v_{th}^p \sigma_{pc}\left(p + n_i e^{\frac{E_i-E}{k_BT}}\right)}\right] + \left[\frac{v_{th}^n v_{th}^p \sigma_{pv}\, \sigma_{nv} g_{vt}^D(E)}{v_{th}^n \sigma_{nv}\left(n + n_i e^{\frac{E-E_i}{k_BT}}\right) + v_{th}^p \sigma_{pv}\left(p + n_i e^{\frac{E_i-E}{k_BT}}\right)}\right] + \left[\frac{v_{th}^n v_{th}^p \sigma_{pg}^a \sigma_{ng}^a g_G^A(E)}{v_{th}^n \sigma_{ng}^a\left(n + n_i e^{\frac{E-E_i}{k_BT}}\right) + v_{th}^p \sigma_{pg}^a\left(p + n_i e^{\frac{E_i-E}{k_BT}}\right)}\right] + \left[\frac{v_{th}^n v_{th}^p \sigma_{pg}^d \sigma_{ng}^d g_G^D(E)}{v_{th}^n \sigma_{ng}^d\left(n + n_i e^{\frac{E-E_i}{k_BT}}\right) + v_{th}^p \sigma_{pg}^d\left(p + n_i e^{\frac{E_i-E}{k_BT}}\right)}\right]\right\} dE$$

where v_{th}^n is the electron thermal velocity and v_{th}^p is the hole thermal velocity, n_i is the intrinsic carrier concentration. σ_{nc} and σ_{ng}^a are the electron capture cross-section for the acceptor states and deep levels with Gaussian distribution respectively. σ_{pc} and σ_{pg}^a are the hole capture cross-sections for the acceptor states and deep levels with Gaussian

distribution respectively and σ_{nv}, σ_{ng}^{d}, σ_{pv}, and σ_{pg}^{d} are the equivalents for donors states.

In the drift-diffusion model, the current densities are expressed in terms of the quasi-Fermi levels ϕ_n and ϕ_p as:

$$\vec{J}_n = -q\mu_n n \nabla \phi_n \quad (4.a)$$

$$\vec{J}_p = -q\mu_p p \nabla \phi_p \quad (4.b)$$

where μ_n and μ_p are the electron and hole mobilities, respectively. The quasi-Fermi levels are then linked to the carrier concentrations and the potential through the two Boltzmann approximations: $n = n_i exp\left(\frac{\psi-\phi_n}{k_B T}\right)$ and $p = n_i exp\left(-\frac{\psi-\phi_p}{k_B T}\right)$ where n_i is the effective intrinsic concentration and T is the lattice temperature.

The electrical characteristics are calculated following the specified physical structure and bias conditions. This is achieved by approximating the operation of the device onto a two dimensional grid, consisting of a number of grid points called nodes. By applying the set of differential equations (Poisson's and continuity equations) onto this grid (or equation's discretisation), the transport of carriers through the structure can be simulated. The finite element grid is used to represent the simulation domain.

Of interest to the present work, the current-voltage characteristics are calculated under illumination and different conditions. In the first case, the CdO film will be considered as a crystalline semiconductor (absence of defects). In the second case, the CdO film will be considered as an amorphous semiconductor, i.e it contains a continuously distributed energy states in its band gap due to the presence of defects.

4.2.1. Crystalline CdO film:

The parameters used in this work, other than those specified in Figure 1, to simulate the Al/n-CdO/p-Si/Al solar cell have are presented in tables 1 and 2 for CdO and Si respectively.

Table 1.

Parameter	Value	Reference
Band gap	2.27 eV	[21, 32]
Electron affinity	4.51 eV	[34]
Donor density, N_D	4.4×10^{19} cm^{-3}	[35, 36]
CB effective density of states, N_C	2.2×10^{19} cm^{-3}	[27]
VB effective density of states, N_V	1.8×10^{19} cm^{-3}	[27]
Electron mobility	7.03 cm^2/Vs	[35]
SRH lifetime for electrons and holes	1×10^{-9} s	[27]

Table 2.

Parameter	Value	Reference
Band gap	1.12 eV	[28]
Electron affinity	4.05 eV	[28]
Acceptor density, N_A	2.0×10^{17} cm^{-3}	Supposed
CB effective density of states, N_C	2.8×10^{19} cm^{-3}	[28]
VB effective density of states, N_V	1.04×10^{19} cm^{-3}	[28]
Electron mobility	1450 cm^2/Vs	[28]
SRH lifetime for electrons and holes	1×10^{-7} s	[27]

The simulated (compared to measured) *J-V* characteristic under AM1.5 spectrum for the ideal Al/n-CdO/p-Si/Al solar cell using the parameters of tables 1 and 2 is shown in figure 2. The short circuit current density (J_{SC}) and the open circuit voltage (V_{OC}) are much higher than those of measured J-V characteristics. The big difference between simulation and measurement is due to the fact that the simulated device is assumed to be perfect free of defects, which is obviously not the case in reality.

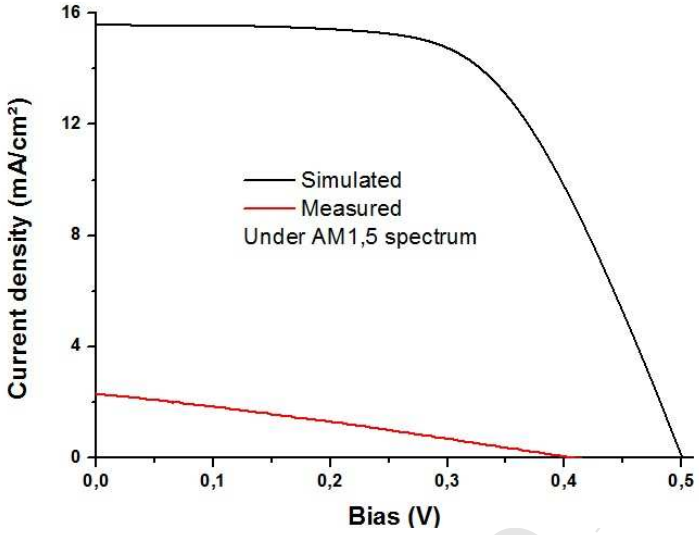

Figure 2.

4.2.2. Amorphous CdO film:

It is well known that, in most cases, thin films have non crystalline structure. It is therefore expected that the polycrystalline or amorphous nature of these films give rise to defects in the film lattice. These will give rise to different types of energy levels in the band gap of the material.

In amorphous semiconductors, the density of states (DOS) is composed of four bands: two tail bands (a donor-like valence band and an acceptor-like conduction band) and two deep level bands (one acceptor-like and the other donor-like). The firsts are modeled as decaying exponentials from the band edge while the latters are modeled using a Gaussian distribution. The density is then given by:

$$g(E) = g_{GA}(E) + g_{GD}(E) + g_{TA}(E) + g_{TD}(E)$$

The subscripts *G* and *T* are for Gaussian and tail respectively while *A* and *D* are for acceptor and donor respectively.

$$g(E) = G_{GA}exp\left[-\left[\frac{E_{GA}-E}{\sigma_D}\right]^2\right] + G_{GD}exp\left[-\left[\frac{E-E_{GD}}{\sigma_D}\right]^2\right] + G_{TA}\,exp\left[\frac{E-E_C}{E_A}\right] + G_{TD}exp\left[\frac{E_V-E}{E_D}\right]$$

Where $E_{V(C)}$is the valence (conduction) band edge, $G_{TD(A)}(\ cm^{-3}eV^{-1})$ the effective density at $E_{V(C)}$, $E_{D(A)}$ the characteristic slope energy of the valence (conduction) band-tail states, $G_{GA(D)}$ the total density ($cm^{-3}eV^{-1}$), $\sigma_D(\sigma_A)$ the standard deviation and $E_{GD(A)}$ the peak energy of the Gaussian distribution.

The parameters of the different constituents of the DOS used to simulate their effect on the Al/n-CdO/p-Si/Al solar cell performance are presented in table 3.

Table 3.

Parameter	Value
Standard deviation of the deep acceptors σ_A (eV)	0.025
Standard deviation of the deep donors σ_D (eV)	0.05
Peak energy of deep acceptors E_{GA} (eV)	1.225
Peak energy of deep donors E_{GD} (eV)	1.225
Characteristic slope energy of the valence band-tail states E_A (eV)	0.1
Characteristic slope energy of the conduction band-tail states E_D (eV)	0.1

Furthermore the capture cross-sections for majority and minority carriers are 1×10^{-14} and $1 \times 10^{-16}\ cm^2$ respectively for all states. Unfortunately it was not possible to find values for these parameters in the literature and therefore default values in the

ACCEPTED MANUSCRIPT

SILVACO TCAD software were used [27]. A schematic representation of such states is shown in figure 3 for densities of: $G_{GA} = G_{GD} = 1 \times 10^{14}\ cm^{-3}eV^{-1}$ and $G_{TA} = G_{TD} = 1 \times 10^{19}\ cm^{-3}eV^{-1}$

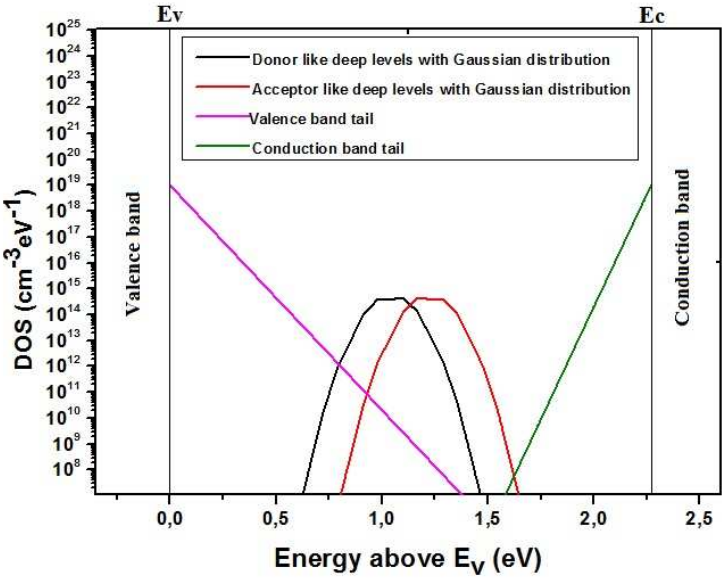

Figure 3.

We will now consider the effect of the different constituents of the DOS on the *J-V* characteristics of the non-ideal Al/n-CdO/p-Si/Al solar cell under AM1.5 spectrum.

a. Effect of the deep levels with Gaussian distribution

First the acceptor-like and donor-like deep level bands in the CdO film are varied symmetrically ($g_{GA}(E) = g_{GD}(E)$) and the *J-V* characteristics of the non-ideal Al/n-CdO/p-Si/Al solar cell under AM1.5 spectrum were computed. The density of tail was kept at a low value at $G_{TA} = G_{TD} = 1 \times 10^{10}\ cm^{-3}eV^{-1}$so that it can be neglected compared to deep states. The acceptor doping concentration of silicon was $N_A = 1 \times$

$10^{18}\ cm^{-3}$. The fixed oxide charge density was also kept low at $Q_f = 3 \times 10^{10}\ cm^{-2}$.

The simulated *J-V* characteristics are shown in Figure 4.

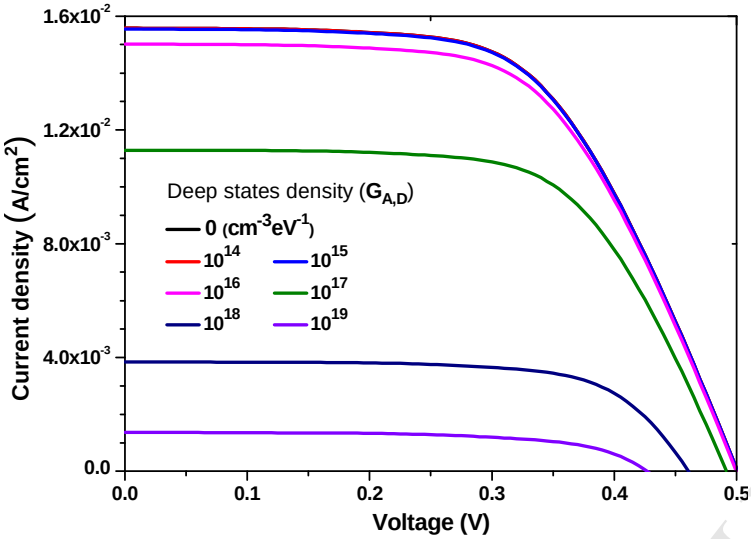

Figure 4.

The figures of merit of the solar cell: the short circuit current density (J_{SC}), the open circuit voltage (V_{OC}), the efficiency (η) and the fill factor (*FF*) are extracted from the *J-V* characteristics. These are shown in figure 5.

ACCEPTED MANUSCRIPT

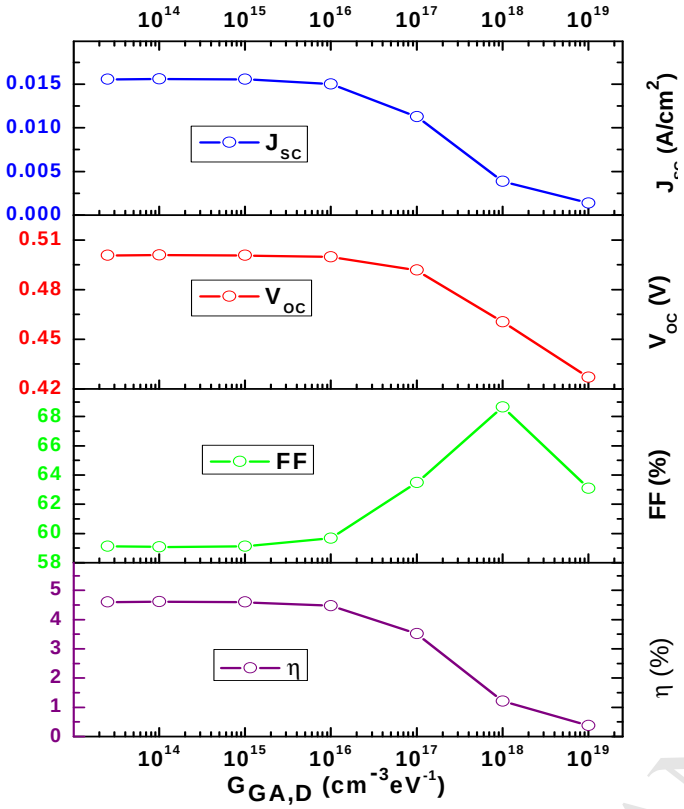

Figure 5.

The cell performance parameters do not change as long as the DOS stays below 1×10^{14} cm^{-3} eV^{-1}. From 10^{16} cm^{-3} eV^{-1}, the presence of deep level bands in the CdO film degrades all solar cell parameters except the fill factor which increases with increasing density. It has to be mentioned that although the decreased parameters tend to approach the real (measured parameters), the fill factor is not. This means that the simulated *J-V* characteristics are not comparable to measurements. The degradation of J_{SC} can be understood from the fact that the photogenerated carriers are captured by dense defects. The degradation of V_{OC} can be explained by a decrease in J_{SC} as well as a possible increase of the dark saturation current J_S of the CdO/Si diode in the presence of defects in accordance to the relation $V_{OC} \approx V_T ln(J_{SC}/J_S)$. The strange behaviuor of the fill factor *FF* (increasing then decreasing) with increasing density of states may be

explained by considering the equivalent circuit of the solar cell. The electric model is often composed of: a diode, representing the behavior of the solar cell in dark, a current source representing the photogenerated current, a series resistance R_s representing the resistive losses of the material and a shunt resistance R_{sh} modeling parasitic currents which cross the cell. When the defect density increases, two cases arise:

(i) If defects are found in the space-charge zone, the increase of the defects DOS can create conduction channels and leakage currents associated. This will decrease R_{sh}.
(ii) If defects are found out of the space charge zone, the increase of the defect DOS will increase the non-radiative recombination rate, thus increasing R_s.
In the present case, ie when the defects density increases, the space charge decreases inducing a decrease in R_{sh} but an increase in R_s. Both resistances are known to influence the fill factor of the solar cell. An increase in R_s (or decrease in R_{sh}) will degrade *FF*. So there is a competition between the effects of both resistances. An increase in *FF* is dominated by the decrease in R_s while a decrease in *FF* is dominated by the decrease in R_{sh}.

b. Effect of the tail states

The second case was studying the effect of the tail states on the solar cell performance by varying, symmetrically, the acceptor and donor densities at the conduction and valence band edges of the CdO film respectively ($G_{TA} = G_{TD}$). The density deep states was kept at a low value of $G_{GA} = G_{GD} = 1 \times 10^{10}\ cm^{-3}eV^{-1}$ so that it can be neglected compared to tail states. The acceptor doping concentration of silicon was $N_A = 1 \times 10^{18}\ cm^{-3}$. The fixed oxide charge density was also kept low at $Q_f = 3 \times 10^{10}\ cm^{-2}$. The simulated *J-V* characteristics are shown in Figure 6.

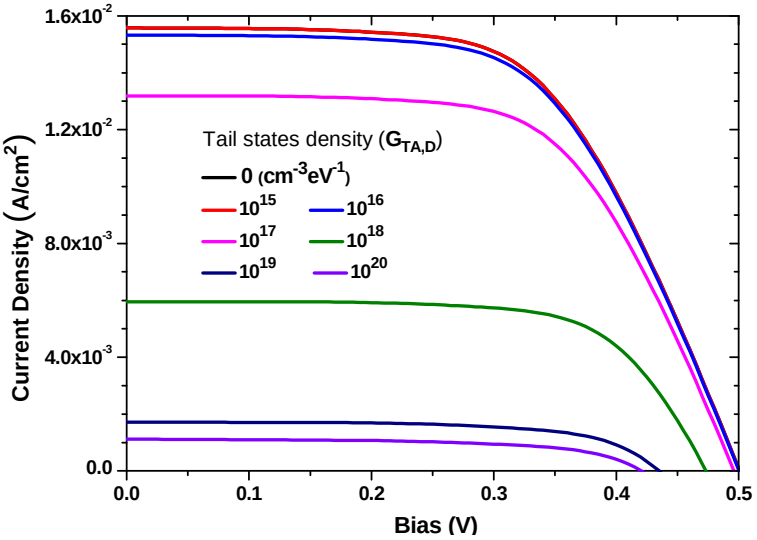

Figure 6.

The figures of merit of the solar cell: the short circuit current density (J_{SC}), the open circuit voltage (V_{OC}), the efficiency (η) and the fill factor (*FF*) are extracted from the *J-V* characteristics. These are shown in figure 7.

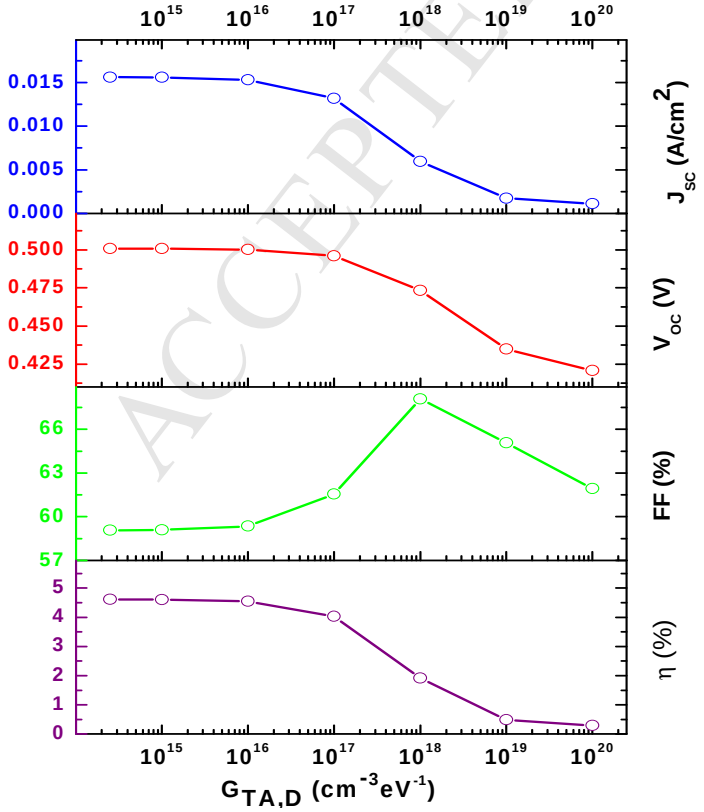

ACCEPTED MANUSCRIPT

Figure 7.

The cell performance parameters do not change as long as the tail states density stays below 1×10^{16} cm^{-3} eV^{-1}. From 10^{16} cm^{-3} eV^{-1}, the presence of deep level bands in the CdO film degrades all solar cell parameters except the fill factor which increases with increasing density until 1×10^{18} cm^{-3} eV^{-1} when it starts to decrease. As in the case of the DOS effect and although the decreased parameters tend to approach the real (measured parameters), the fill factor is not. This means that the simulated *J-V* characteristics are still not comparable to measurements.

It has to be mentioned that the effect of tail states is very similar to that of Deep levels with Gaussian distribution. In both cases the effect indicates that the defects act as dopants, modifying the doping profile and reducing the space charge zone of the junction. So the same analysis of the dependence of the solar cell parameters on the density of the tail states used in the previous case may are applicable here.

c. Effect of p-type doping of silicon:

The third and last case studied is the effect of the p-type doping of the silicon absorber layer (Si) which was varied from $N_A = 2.5 \times 10^{17}$ to $1 \times 10^{18}\ cm^{-3}$. The other parameters were: the density of the Gaussian deep states distribution $G_{A,D} = 1 \times 10^{15} cm^{-3} eV^{-1}$, the density of the tail $G_{TA,D} = 1 \times 10^{19} cm^{-3} eV^{-1}$ and the fixed oxide charge density $Q_f = 1 \times 10^{10} cm^{-2}$. The simulated *J-V* characteristics are shown in Figure 8.

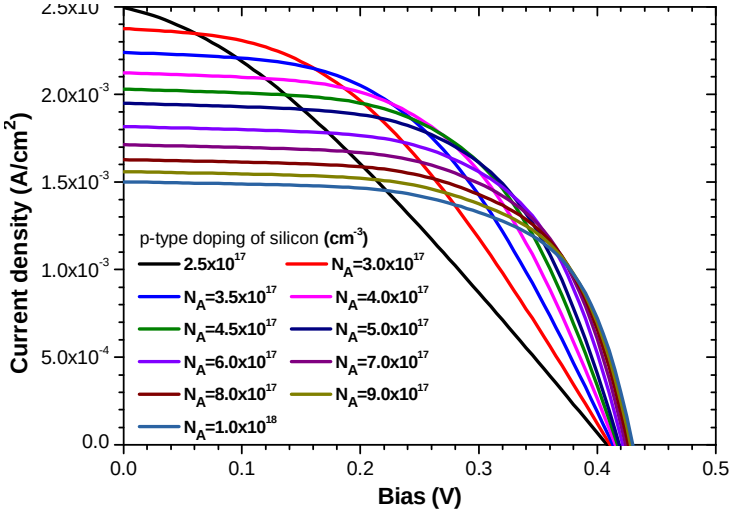

Figure 8.

The extracted figures of merit of the solar cell are shown in figure 9 under the effect of variable p-type doping of silicon.

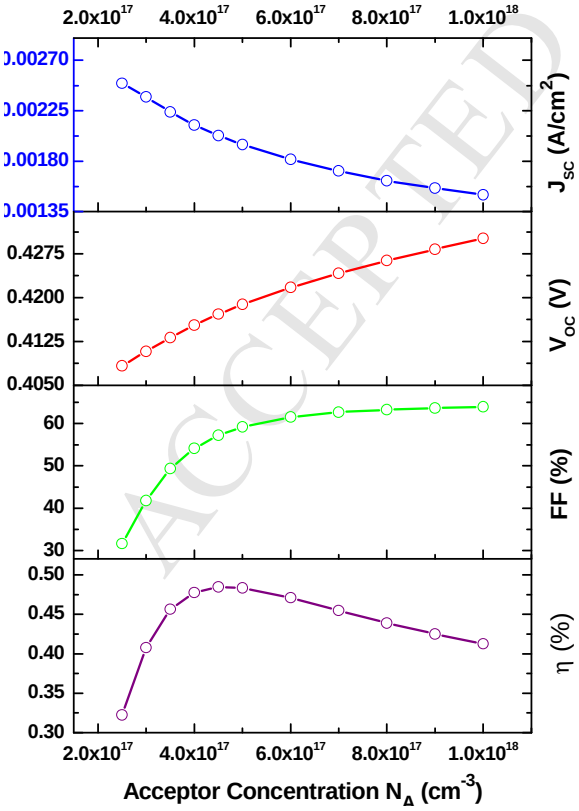

Figure 9.

ACCEPTED MANUSCRIPT

V_{OC} increases with increasing p-type doping of Si. This can be understood bearing in mind that it is proportional to the barrier (diffusion, built-in) voltage (V_B) of the p-n junction and the latter is proportional to the doping density of the two sides of the junction as $V_B = kT/qln(N_A N_D/n_i^2)$. J_{SC}, on the other hand, decreases which may be due to the decrease in of the junction dark saturation current density J_S which in turn is inversely proportional to the doping density. This relationship is given by $J_{SC} = J_S ln(V_{OC}/V_T) \propto (1/N_A) ln(V_{OC}/V_T)$. Although V_{OC}increases, but the increase of N_A (the decrease of $1/N_A$) will be far more influent. The increase in the fill factor (*FF*) with increasing N_A may be interpreted by the effect on the space charge region (SCR) of which the width increase with decreasing doping density. This may create a path through the defects in SCR which is usually represented as a shunt resistance R_{sh} in the electrical model of a diode. The effect of R_{sh} on *FF* is well known: they are simply proportional. Thus a decrease in R_{sh} induces a decrease in *FF*.

d. Simulation of the effect of illumination power intensity on the Al/ n-CdO/ p-Si/Al solar cell

Simulation of the effect of the tail and Gaussian defect on the Al/ n-CdO/ p-Si/Al solar cell has lead to comparable values between simulation and measurement for both $V_{OC}$and J_{SC}. However the effect was not able to obtain comparable values for *FF*. The acceptor doping of silicon induced comparable values for *FF*. Combing the effects of defects in CdO and doping in Si, all parameters were almost perfectly reproduced when the solar cell is subjected to AM1.5 spectrum (light power intensity of 100 mW/cm^2). The values which gave comparable simulation and measurement were: an acceptor p-type doping of silicon, N_A= 2.07x10^{17} cm^{-3}, a total density of the Deep levels with

Gaussian distribution, $G_{Ga,d}$=1x10^{15} cm^{-3}/eV, a density of tail states, $G_{Ta,d}$= 1.5x10^{19} cm^{-3}/eV, and a fixed oxide charge density; Qf=5x10^{11} cm^{-2}. These values were then used to simulate the effect of light intensity on the *J-V* characteristics of the solar cell and compared to measurements. This comparison is shown in figure 10.

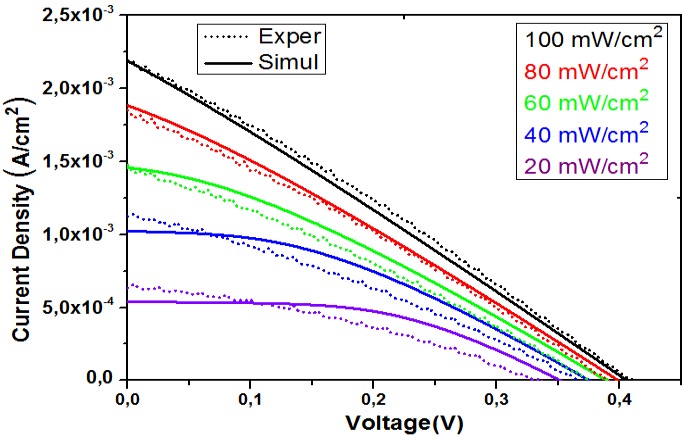

Figure 10.

As it is very clear there is a very good agreement between simulation and measurements. From figure 10, the solar cell parameters are extracted and presented in figure 11. The extracted parameters give almost a perfect match between simulation and measurement.

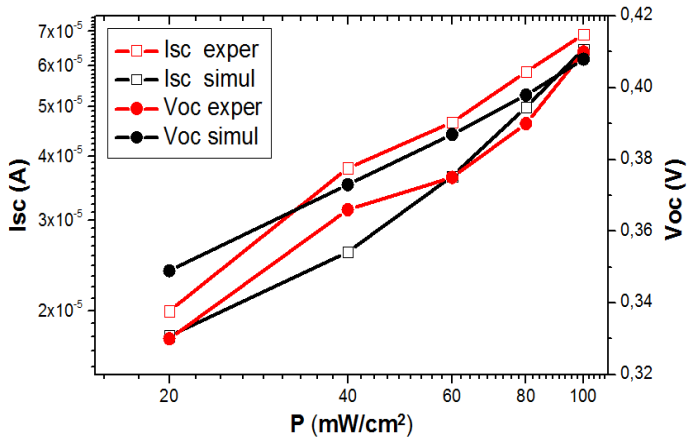

Figure 11.

5. Conclusion

An n-CdO/p-Si heterojunction solar cell which was fabricated by sol–gel method. Optical characterisation showed a very poor performance [21]. In this work numerical simulation using Silvaco ATLAS software is used to model the aforementioned solar cell and to elucidate this poor performance. Several possible causes were considered: the presence of defects in the semiconductor (tail or Deep levels with Gaussian distribution), fixed charge, and doping of silicon. The defects were found to mainly affect V_{OC} and J_{SC}. On the other hand *FF* is mainly affected by the p-type doping of silicon. Good comparison between experimental and simulation results was obtained with these values: an acceptor p-type doping of silicon, N_A= 2.07x10^{17} cm^{-3}, a total density of the Deep levels with Gaussian distribution, $G_{Ga,d}$=1x10^{15} cm^{-3}/eV, a density of tail states, $G_{Ta,d}$= 1.5x10^{19} cm^{-3}/eV, and a fixed oxide charge density; Qf=5x10^{11} cm^{-2}. These values produced a good agreement between simulated and measured *J-V* characteristics of the solar cell under the effect of the light power intensity.

6. References

[1] Chandiramouli R. Jeyaprakash B G. Review of CdO thin films.Solid State Sciences 2013; 16: 102-10.

[2] Cristaldi D A. Millesi S. Crupi I. Impellizzeri G. Priolo F. Jacobs R M J. et al. Structural, Electronic, and Electrical Properties of an Undoped n-Type CdO Thin Film with High Electron Concentration. J Physical Chemistry C 2014; 118: 15019-26.

ACCEPTED MANUSCRIPT

[3] Gomez Daza O, Arias-Carbajal Readigos A, Campos J, Nair M T S, Nair P K. Formation of conductive CdO thin films on photoconductive CdS thin films for window layer applications in solar cells. Mod Phys Lett B 2001; 15: 609-12.

[4] Durandurdu M. Atomic structure of amorphous CdO from first principles simulations. Journal of Non-Crystalline Solids 2015; 412, 15: 11-5

[5] Cimino A. Marezio M. Lattice parameter and defect structure of cadmium oxide containing foreign atoms, J. Phys. Chem. Solids 1960; 17: 57-64.

[6] Haul R. Just D. Disorder and oxygen transport in cadmium oxide, J. Appl. Phys 1962; 33: 487-93.

[7] King P.D.C. Veal T.D. Jefferson P.H. Zúñiga-Pérez J. Muñoz-Sanjosé V. McConville C.F. Unification of the electrical behavior of defects, impurities, and surface states in semiconductors: virtual gap states in CdO. Phys Rev B 2009; 79: 035203(1-5).

[8] Dakhel A A. Optical and electrical properties of copper-doped and nano-crystallite CdO thin films. Solid State Sciences 2014; 31: 1-7.

[9] Zhu Y. Mendelsberg R J. Zhu J. Han J. Anders A. Dopant-induced band filling and bandgap renormalization in CdO:In films. J Phys D: Appl Phys 2013; 46: 195102.

[10] Dakhel A A. Improving carriers mobility in copper and iron-codoped CdO. Materials Science in Semiconductor Processing 2014; 17: 194–198.

[11] Zhao Z, Morel D L, Ferekides C S. Electrical and optical properties of tin-doped CdO films deposited by atmospheric metalorganic chemical vapor deposition. Thin Solid Films 2002; 413: 203-11.

[12] Yan M, Lane M, Kannewurf C R, Chang R P H. Highly conductive epitaxial CdO thin films prepared by pulsed laser deposition. Appl Phys Lett 2001, 78: 02342.

[13] Carballeda-Galicia D M, Castanedo-Perez R, Jimenez-Sandoval O, Jimenez-Sandoval S, Torres-Delgado G, Zuniga-Romero C I. High transmittance CdO thin films obtained by the sol-gel method. Thin Solid Films 2000, 371: 105-8.

[14] Subramanyam T K. Uthanna S. Naidu B S. Preparation and characterization of CdO films deposited by dc magnetron reactive sputtering. Mater Lett 1998; 35: 214-20.

[15] Lokhande B J. Patil P S. Uplane M D. Studies on cadmium oxide sprayed thin films deposited through non-aqueous medium. Mater. Chem Phy 2004; 84: 238-40.

[16] Deokate R J. Lokhande C D. Liquefied petroleum gas sensing properties of sprayed nanocrystalline Ga-doped CdO thin films. Sensors and Actuators B 2014; 193: 89– 94.

[17] Cui G. Li Z. Gao L. Zhang M. CdO nanosheet film with a (200)-preferred orientation with sensitivity to liquefied petroleum gas (LPG) at low-temperatures. Phys Chem Chem Phys 2012; 14: 16321–5.

[18] Ismail R A. Al-Samarai A M E. Mohmed S J. Ahmed H H. Characteristics of nanostructured CdO/Si heterojunction photodetector synthesized by CBD. Solid-State Electronics 2013; 82: 115–21.

[19] Karatas S. Yakuphanoglu F. Amanullah FM. Capacitance–voltage and conductance–voltage characteristics of Ag/n-CdO/p-Si MIS structure prepared by sol–gel method. Journal of Physics and Chemistry of Solids 2012; 73: 46–51.

[20] Su L M, Grote N, Schmitt F. Diffused planar InP bipolar transistor with a cadmium oxide film emitter. Electron Lett 1984; 20: 716-7.

[21] Yakuphanoglu F. Nanocluster n-CdO thin film by sol-gel for solar cell applications. Applied Surface Science 2010; 257: 1413-9.

[22] Ismail R A. Abdulrazaq O A. A new route for fabricating CdO/c-Si heterojunction solar cells. Sol Energy Mat Solar Cells 2007; 91: 903-7.

[23] Zaien M. Ahmed N.M. Hassan Z. Fabrication and characterization of nanocrystalline n-CdO/p -Si as a solar cell. Superlattices and Microstructures 2012; 52: 800–6.

[24] Zaien M. Ahmed N.M. Hassan Z. Fabrication and Characterization of an n-CdO/p-Si Solar Cell by Thermal Evaporation in a Vacuum. Int J Electrochem Sci 2013; 8: 6988–96.

[25] Murali K.R. Kalaivanan A. Perumal S. Neelakanda Pillai N. Sol–gel dip coated CdO:Al films. J Alloys and Compounds 2010; 503: 350–3.

[26] Zou B S. Volkov V V. Wa Z L. Optical Properties of Amorphous ZnO, CdO, and PbO Nanoclusters in Solution. Chem Mater 1999, 11: 3037-43.

[27] SILVACO-TCAD, ATLAS User's Manual: Device simulation software. SILVACO International, California: 2013.

[28] Sze S. M. Physics of Semiconductor Devices. 2nd edition. New York: John Wiley and Sons; 1982

[29] Schockley W. Read W T. Statistics of the recombination of holes and electrons. Phys Rev 1952, 87: 835.

[30] Hall R N. Eletron-hole recobination in germanium. Phys Rev 1952, 87: 387.

[31] Zeman M. van den Heuvel J. Kroon M. Willemen J. Amorphous Semiconductor Analysis (ASA) User's Manual. Version 3.3. Delft Univ. of Technology, Delft: 2000.

[32] Dakhel A A. Optoelectronic properties of hydrogenated Dy-doped CdO films. Eur Phys J Appl Phys 2009; 45: 20303 (5pp.).

[33] Meftah AM. Meftah AF. Hiouani F. Merazga A. Numerical simulation of the defect density influence on the steadystate response of a silicon-based p–i–n cell. J Phys: Condens Matter 2004; 16: 2003–16.

ACCEPTED MANUSCRIPT

[34] Yakuphanoglu F. Caglar M. Caglar Y. Ilican S. Electrical characterization of nanocluster n-CdO/p-Si heterojunction diode: J Alloys Compd 2010; 506: 188-93.

[35] Dakhel A. A. Effect of tellurium doping on the structural, optical, and electrical properties of CdO. Sol Energy 2010; 84: 1433-8.

[36] Henríquez R. Grez P. Muñoz E. Dalchiele E A. Marotti R E. Gómez H. Template-free non-aqueous electrochemical growth of CdO nanorods. Thin Solid Films 2011; 520: 41-6.

ACCEPTED MANUSCRIPT

ACCEPTED MANUSCRIPT

Figure captions

Figure 1. A two dimensional schematic representation of the cross-section of the Al/ n-CdO/ p-Si/Al diode.

Figure 2. Comparison simulated and measured *J-V* characteristics of the ideal Al/n-CdO/p-Si/Al solar cell under AM1.5 spectrum.

Figure 3. The density of states (deep Gaussian and tail) in the energy gap of CdO.

Figure 4. The simulated *J-V* characteristics of the non ideal Al/n-CdO/p-Si/Al solar cell under AM1.5 spectrum for variable acceptor-like and donor-like deep Deep levels with Gaussian distribution in the CdO film.

Figure 5. The effect of deep level Gaussian staes in the CdO film on the solar cell performance parameters under AM1.5 spectrum.

Figure 6. The simulated *J-V* characteristics of the non ideal Al/n-CdO/p-Si/Al solar cell under AM1.5 spectrum for variable acceptor-like and donor-like deep tail states in the CdO film.

Figure 7. The effect of the density of the tail states at the conduction and valence band edges in the CdO film on the solar cell performance parameters under AM1.5 spectrum.

Figure 8. The simulated *J-V* characteristics of the non ideal Al/n-CdO/p-Si/Al solar cell under AM1.5 spectrum for variable p-type doping of silicon $N_A = 2.5 \times 10^{17}$ to $1 \times 10^{18}\ cm^{-3}$. The other parameters were: the density of the Gaussian deep states distribution $G_{A,D} = 1 \times 10^{15} cm^{-3} eV^{-1}$, the density of the tail $G_{TA,D} = 1 \times 10^{19} cm^{-3} eV^{-1}$ and the fixed oxide charge density $Q_f = 1 \times 10^{10} cm^{-2}$.

Figure 9. The extracted figures of merit extracted from the simulated *J-V* characteristics of the non ideal Al/n-CdO/p-Si/Al solar cell under AM1.5 spectrum for variable p-type doping of silicon $N_A = 2.5 \times 10^{17}$ to $1 \times 10^{18}\ cm^{-3}$.

Figure 10. Comparison of simulated and measured [21] *J-V* characteristics of the Al/ n-CdO/ p-Si/Al solar cell diode for different illumination power intensities.

Figure 11. Comparison of the Al/ n-CdO/ p-Si/Al solar cell parameters extracted from the simulated and measured [21] *J-V* characteristics of figure 11 for different illumination power intensities.

ACCEPTED MANUSCRIPT

ACCEPTED MANUSCRIPT

Table captions

Table 1. Parameters used to simulate the CdO film of the ideal Al/n-CdO/p-Si/Al solar cell.

Table 2. Parameters used to simulate silicon of the ideal Al/n-CdO/p-Si/Al solar cell.

Table 3. Parameters of the DOS used to simulate the CdO film of the Al/n-CdO/p-Si/Al solar cell.

ACCEPTED MANUSCRIPT